FIELD DEPENDENCE ON MOBILITY IN COPPER AND LEAD CHALCOGENIDE BASED QUANTUM DOT SENSITIZED SOLAR CELLS

Abstract

This chapter discusses the fabrication of quantum dot sensitized solar cells of Copper Sulphide, Copper Tin Sulphide, Copper Zinc Tin Sulphide and Lead Tin Sulphide. These quantum dot sensitized solar cells were analysed using SCLC (Space Charge Limited Conduction) method and further simulation was also made using SCAPS-1D software

Author

Maya Mathew
Department of Physics
Payyannur College
Kannur, Kerala, India

KC Preetha
Principal
Sree Narayana College
Varkala Trivandrum, India
kcpreetha1990@gmail.com

I. INTRODUCTION

Conventional p-n junction solar cells were fast replaced by dye sensitized solar cells [1-3] and currently by quantum dot sensitized solar cells [4-6]. The characteristics exclusive of quantum dots such as the multiple electron generation and high absorption coefficient are the prime factors that influence the performance of such solar cells [7]. In quantum dot sensitized solar cells, quantum dots coated onto some high band gap semiconductor is used as the photo anode and the polysulphide mixture is the commonly used electrolyte. Electrons generated in the photo anode when illuminated pass through the wide bandgap semiconductor and finally to the external circuit. The electrons lost are regenerated by the oxidation/ reduction processes of the electrolyte [8]. The electron transfer in quantum dot sensitized solar cells may be hindered owing to the organic surfactant used for the confinement of quantum dots. Studies have been made for the usage of short ligands as capping agents to enhance electron transfer [9, 10].

Mobility of charge carriers is an important factor for the efficiency of solar cells. Usually the charge carrier mobility is calculated from the carrier concentration measured. But in certain cases, when the injected charge carriers create an electric field inside the device, the mobility become dependent on the field created, which is the steady state space charge limited conduction (SS-SCLC). A recent work of Bhattarai at.al. found that there is a dependence of mobility on the type of electric field. In order to avoid errors, the authors have suggested to take a plot of $V^{1/2}$ versus $\log(J/V^2)$ where a straight line will be obtained if there is space charge limited current. Also a positive slope will be obtained for positive field dependence and a negative slope for negative field dependence. From the values of the slope and intercept obtained, the mobility of charge carriers can be determined   [11- 14].

There are few works in literature on the fabrication of copper tin sulphide quantum dot sensitized solar cells. We have, for the first time, fabricated cost effective quantum dot sensitized solar cells using copper tin sulphide, copper sulphide and copper zinc tin sulphide as the sensitizer materials by cost effective Successive Ionic Layer Adsorption and Reaction (SILAR) technique. This chapter reports the negative field dependence in these solar cells and the calculation of mobility using the SS- SCLC method.

II. EXPERIMENTAL

Fabrication of quantum dot sensitized solar cells: For the fabrication of quantum dot sensitized solar cells, both photo anode and photocathode were prepared on indium doped tin oxide (ITO) substrates of resistivity less than 20 Ω/cm^2. Here, graphite coated on ITO substrate was used as the photocathode. A layer of TiO_2 was coated onto the ITO substrate using doctor blade technique and annealed it at $60^{\circ}C$ for two hours. Quantum dots of ternary and quaternary copper and lead chalcogenides coated onto TiO_2 layer using 5 SILAR cycles and quantum dots of copper sulphide coated using 10 SILAR cycles were used as the photo anode. The dipping and rinsing time was set as 1 minute and 2 seconds respectively. The SILAR procedure followed has been mentioned in our previous paper [15]. Table7.1 shows the details of the deposition of the sensitizer material, deposition technique, precursors used and their ratios. After coating with the sensitizer material, the photo anodes were air dried. The solar cell was assembled after adding few drops of the electrolyte KI_3/I_3^- between the

photocathode and the photo anode. CTS quantum dot sensitized solar cell and its electrodes has been shown in figure 1.

Table 1: Details of the fabricated solar cells

| Sl No.	Solar cell	Sensitizer	Millimolar Precursors used	Ratio of precursors taken.
1.	ITO/TiO$_2$/Cu$_2$S QDs/ KI$_3$/I$_3^-$ /Graphite/ITO	Cu$_2$S QDs	CuCl$_2$.2H$_2$O and Na$_2$S along with 0.1ml of TEA as complexing agent for cation.	2:1
2.	ITO/TiO$_2$/Cu$_2$SnS$_3$ QDs/KI$_3$/I$_3$/Graphite/ITO	Cu$_2$SnS$_3$ QDs	CuCl$_2$.2H$_2$O, SnCl$_2$.2H$_2$O and Na$_2$S along with 0.1ml of TEA	2:1:3
3.	ITO/TiO$_2$/Cu$_2$ZnSnS$_4$ QDs/KI$_3$/I$_3$/Graphite/ITO	Cu$_2$ZnSnS$_4$ QDs	CuCl$_2$.2H$_2$O, ZnCl$_2$.2H$_2$O, SnCl$_2$.2H$_2$O and Na$_2$S along with 0.1ml of TEA	2:1:1:4
4.	ITO/TiO$_2$/PbSnS$_2$ QDs/ KI$_3$/I$_3^-$/Graphite/ITO	PbSnS$_2$ QDs	Pb(CH$_3$COO)$_2$, SnCl$_2$.2H$_2$O and Na$_2$S alongwith0.1ml of TEA	1:1:2
5.	ITO/TiO$_2$/Pb$_2$ZnSnS$_4$ QDs/ KI$_3$/I$_3^-$/Graphite/ITO	Pb$_2$ZnSnS$_4$ QDs	Pb(CH$_3$COO)$_2$, ZnCl$_2$.2H$_2$O, SnCl$_2$.2H$_2$O and Na$_2$S along with 0.1ml of TEA	2:1:1:4
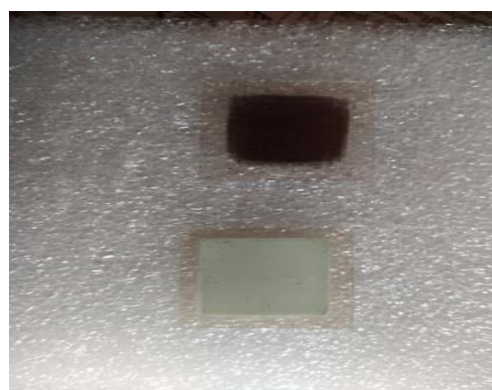
Figure 1 : CTS quantum dot sensitized solar cell and its electrodes

Characterization of the quantum dot sensitized solar cells: The current- voltage relation was measured using Keithley Source meter 2400 and Xenon lamp, set at the standard

illumination of 1sun. The quantum dot sensitized solar cells were tested at 1000 W/m^2 while the solar cells of Cu_2S and $PbSnS_2$ were also tested at low illumination of 1.2 mW/cm^2. The data pertaining to I-V curve were obtained and the efficiency of the solar cells was found manually by plotting the data in Origin software.

III. RESULTS AND DISCUSSION

1. **Synthesis and Characterization of Copper Sulphide quantum dot thin films and J-V characteristics of its solar cells:** The Cu_2S quantum dot thin films coated were characterized using X-ray diffraction and the diffraction pattern is shown in figure 2. The cross-sectional SEM image of Cu_2S quantum dot thin film is shown in figure 3.
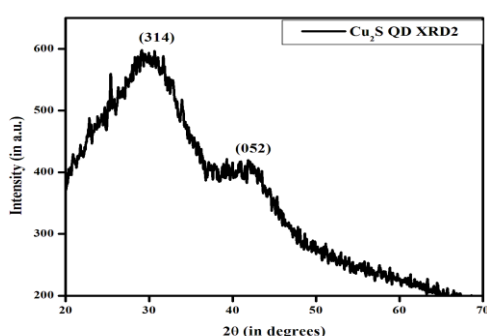

Figure 2: XRD pattern of Cu₂S quantum dot thin film
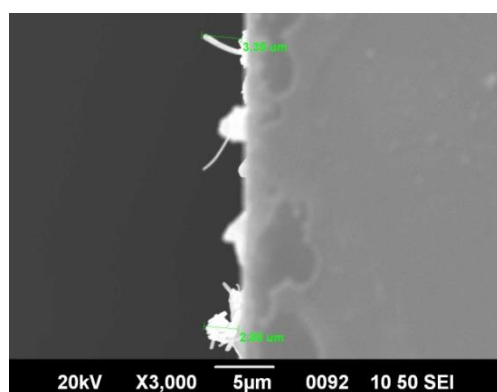
Figure 3: SEM image of Cu₂S quantum dot thin film

The diffraction pattern matched well with the standard pattern for Cu_2S given by PDF 65-3816. Broad peaks, indicating nanosized particles, were observed at 29° and 42° corresponding to the diffraction from (314) and (052) crystal planes. The crystallite size, lattice strain and dislocation density were calculated from the most preferred orientation, using standard equations [16] and are tabulated in table 2. The value of crystallite size confirms that quantum dots are formed.

Table 2: Crystal parameters of Cu₂S quantum dot thin films

Sample	2θ	FWHM	Crystallite size	Lattice strain	Dislocation density
Cu₂S XRD2	29.4	0.1935	0.740 nm	0.1844	1.826

An efficiency of 4.91% was achieved for Cu_2S quantum dot sensitized solar cell under low illumination as shown in the J-V characteristics in figure 4.
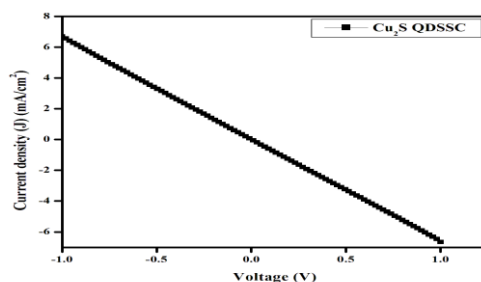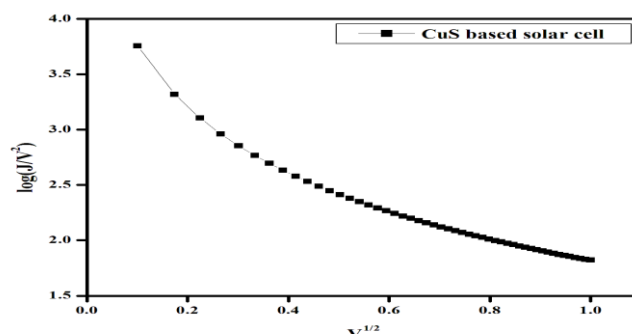
Figure 4: J-V curve of Cu₂S sensitized solar cell

The solar cell parameters have been tabulated in table 3. On plotting the $V^{1/2}$ – $\log(J/V^2)$ graph, (figure 5) a straight line was obtained indicating the SCLC regime and it had a negative slope due to negative field dependence. Mobility of charge carriers was calculated from the intercept and slope and it was found to be $1.912 \times 10^{-3} cm^2/Vs$.

Table 3: Solar cell parameters of ITO/TiO₂/Cu₂S QDs/ KI₃/I₃⁻/Graphite/ITO quantum dot sensitized solar cells

Solar cell	Voc	Jsc	FF	η
ITO/TiO₂/ Cu₂S QDs/ KI₃/I₃⁻/Graphite/ITO	1 V	6.742 mA/cm²	0.7288	4.91%

Figure 5: Negative field dependence of SCLC region for Cu₂S sensitized solar cell

2. **Synthesis and Characterization of Copper Tin Sulphide quantum dot thin films and J-V characteristics of its solar cell:** The copper tin sulphide (CTS) quantum dot thin films were characterised using X-ray diffraction and the diffraction pattern is shown in figure 6. The crystallite size has been calculated from Scherrer equation and it has been tabulated in table 4.
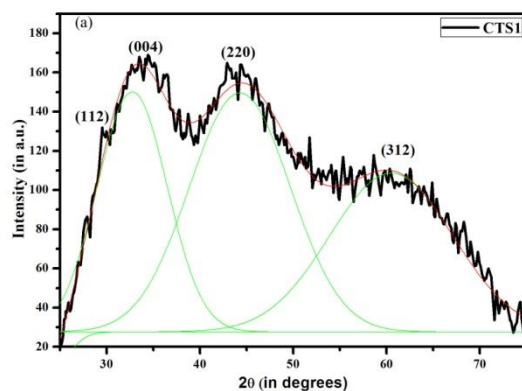
Figure 6: XRD pattern of CTS quantum dot thin film

Table 4: Particulars of crystallites of CTS

Specimen	2theta	FWHM (in rad)	Crystallite size (in nm)	Lattice strain	Dislocation density
CTS	34.5	0.467	0.311	0.376	10.339

The bandgap has been calculated from its Tauc plot which has been shown in figure 7. Due to quantum confinement, there are multiple bandgaps and they have been tabulated in table 5.
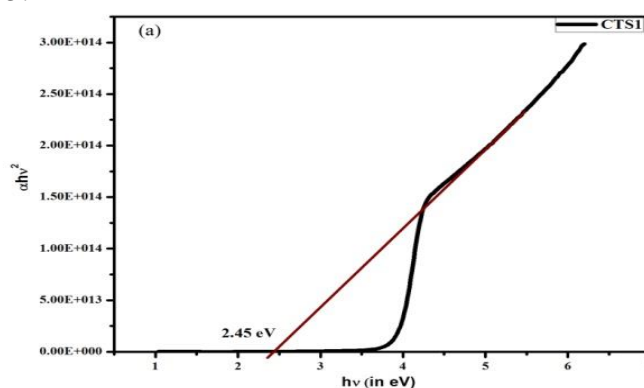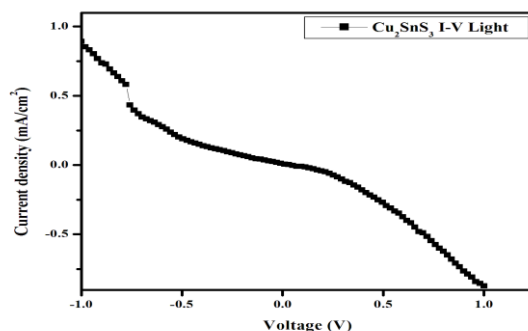

Figure 7: Tauc plot of CTS

Table 5: Band gap and absorption threshold of CTS

Sample	Absorption maximum	Bandgap	
		1Se- 1Sh	1Pe- 1Ph
CTS	282 nm	2.45 eV	4.0 eV

The J-V characteristic of CTS quantum dot sensitized solar cell at standard illumination of 1000 W/m^2 is shown in figure 7.8. The solar cell parameters have been tabulated in table 6.
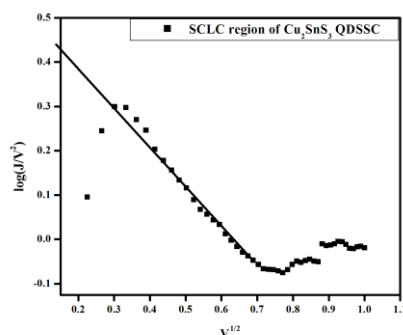
Figure 8: J-V characteristic of CTS quantum dot sensitized solar cell

Table 6: Solar cell parameters of ITO/TiO₂/Cu₂SnS₃ QDs/ KI₃/I₃⁻/Graphite/ITO quantum dot sensitized solar cell

Solar cell	Voc	Jsc	FF	η
ITO/TiO$_2$/Cu$_2$SnS$_3$ QDs/ KI$_3$/I$_3^-$/Graphite/ITO	1 V	0.885 mA/cm^2	0.229	0.203%

The solar cell was also found to have negative field dependence in the space charge conduction regime. The plot of $V^{1/2} – \log(J/V^2)$ showed a negative slope as shown in figure 7.9 and mobility was calculated to be 5.099 X 10^{-4} cm^2/Vs.

Figure 9: Negative field dependence in CTS quantum dot sensitized solar cell

3. **Synthesis and Characterization of Copper Zinc Tin Sulphide quantum dot thin films and and J-V characteristics of its solar cell:** The XRD pattern of CZTS quantum dot thin film is shown in figure 10. The XRD pattern matches well with the wurtzite phase of copper zinc tin sulphide [17]. There is one major peak at 29.87° and a minor peak at 41.6° which corresponds to the diffractions due to (002) and (102) planes respectively. The peaks are slightly shifted owing to lattice strain as a consequence of quantum confinement. The peak at 40° is absent in the case of kesterite phase and so it is a differentiating factor between the kesterite and wurtzite phases. The parameters such as crystallite size, lattice strain and dislocation density were calculated from the most preferred orientation. The crystallite size was calculated using the Debye- Scherrer formula and it has been found to be 0.72nm. The crystallite size is within the Bohr radius for CZTS [18] and so the quantum dots are in the strong confinement regime. Also the

lattice strain and dislocation density have been calculated and alongwith crystallite size, the values have been tabulated in table 7. As the size of the particles is nanosized, the lattice strain and dislocation density values are very high.
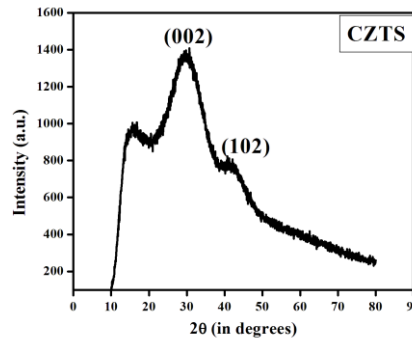

Figure 10: XRD pattern of wurtzite Cu_2ZnSnS_4 quantum dots

**Table 7: Crystal parameters of wurtzite CZTS quantum dot thin films**

Most preferred orientation	FWHM (radians)	Crystallite size	Lattice Strain	Dislocation density
(002)	0.1926	0.720 nm	10.582	1.929 nm^{-2}

Figure 11 (a) shows the plot of absorption coefficient against wavelength for CZTS quantum dot thin film. The quantum dot thin film has very high absorption coefficient of the order of 10^6 m^{-1} in the ultraviolet region i.e. from 300nm to 400 nm and an absorption coefficient of 10^4 m^{-1} in the visible and near infra red regions. The high absorption coefficient of CZTS quantum dot thin film makes it a potential candidate in photovoltaics. There are multiple absorption peaks owing to highly confined structure. The bandgap was determined from Tauc plot and it was found to be 3.81 eV, corresponding to 1Se-1Sh transition.


(a)
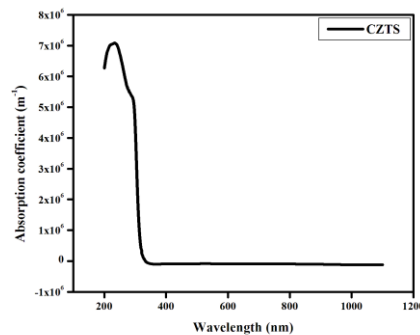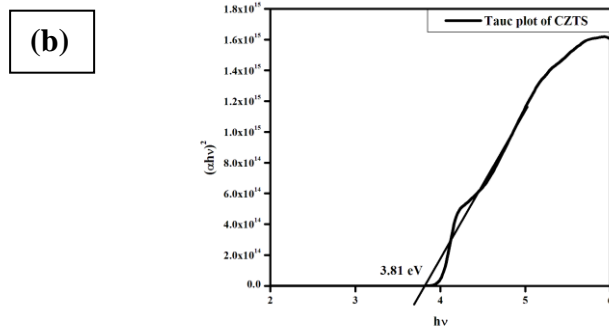
Figure 11: (a) Absorption coefficient and (b) Tauc plot of CZTS quantum dot thin film

Cross – sectional Scanning Electron Microscopy (SEM) images were taken to determine the thin film thickness and it has been shown in figure 7.12. Good quality uniformly coated thin film can be viewed from the image. An average film thickness of 508.85nm has been determined from the SEM image.
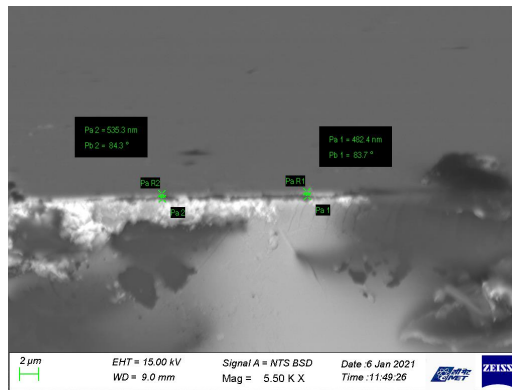
Figure 12: Cross- sectional SEM image of CZTS quantum dot thin film

Hall measurement was performed on the sample and the CZTS quantum dot thin film was found to be p-type in nature with hole mobility of 1.549×10^2 cm²/Vs, bulk concentration of 3.348×10^{12} cm⁻³ and average Hall coefficient of 1.84×10^6 cm³/C.

J- V characteristics of CZTS sensitized solar cell is shown in figure 13 and the solar cell parameters are tabulated in table 8. Good efficiency of 0.311% has been achieved.
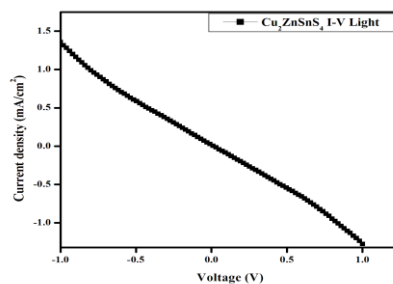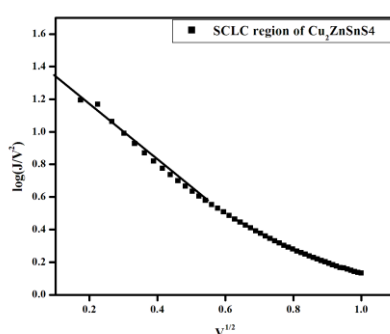

Figure 13: J-V curve of CZTS sensitized solar cell

Table 8: Solar cell parameters of ITO/TiO$_2$/Cu$_2$ZnSnS$_4$ QDs/ KI$_3$/I$_3^-$/Graphite/ITO quantum dot sensitized solar cell

Solar cell	Voc	Jsc	FF	η
ITO/TiO$_2$/ Cu$_2$ZnSnS$_4$ QDs/ KI$_3$/I$_3^-$/Graphite/ITO	1 V	1.359 mA/cm^2	0.229	0.311%

This solar cell also has negative field dependence in the space charge limited conduction regime as shown in figure 14. From the negative slope, the mobility was calculated as 3.774×10^{-4} cm^2/Vs.

Figure 14: Negative field dependence of SCLC region for CZTS sensitized solar cell

4. **Synthesis and Characterization of Lead Tin Sulphide quantum dot thin films and J-V characteristics of its solar cell:** The XRD pattern of PTS quantum dot thin film is shown in figure 7.15. The pattern matches well with the cubic phase of lead tin sulphide [19]. One peak corresponding to the diffraction from (212) plane is from orthorhombic phase. The crystallite size, lattice strain and dislocation density were calculated for both the cubic and orthorhombic phase and it has been tabulated in table 7.9. The values given in bold are that of orthorhombic phase. The lattice strain and dislocation density values are higher for the orthorhombic phase as the crystallite size of the former is smaller.
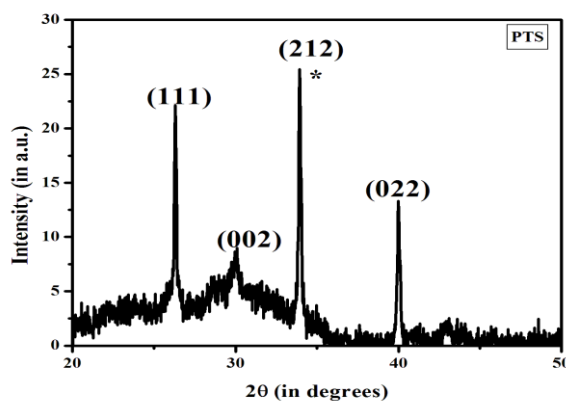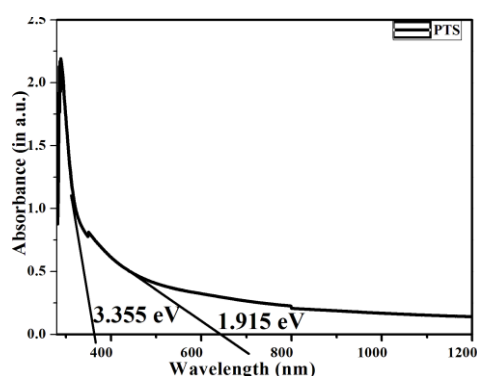

Figure 15: XRD pattern of PTS quantum dot thin film
**Table 9: Structural parameters of PbSnS$_2$**

Sample	2θ (°)	Hkl	D (nm)	Lattice strain	Dislocation density (nm^{-2})
PbSnS$_2$	26.3	(111)	44.526	0.0034	0.0005
	33.93	**(212)**	**55.290**	**0.0021**	**0.0003**

Due to the presence of direct bandgap, the bandgaps can be found simply by drawing tangent from the absorption edge to the x-axis figure 7.16. There are multiple bandgaps owing to quantum confinement.

Figure 16: Absorption spectrum and bandgaps of PbSnS$_2$ quantum dot thin films

The J-V characteristics of PTS quantum dot sensitized solar cell is shown in figure 17 and it has been found that the solar cell yields efficiency of 0.031% under low illumination of 1.2mW/cm^2. The solar cell parameters are shown in table 10.
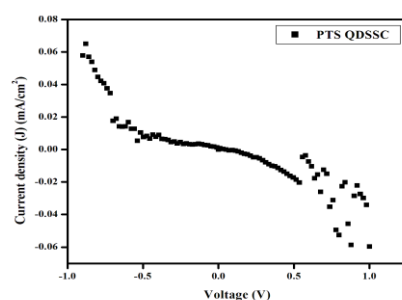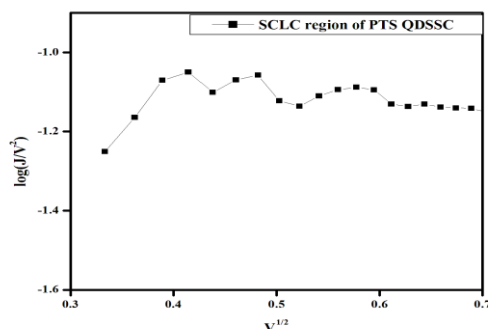

Figure 17: J-V curve of PTS sensitized solar cell

Table 10: Solar cell parameters of ITO/TiO$_2$/PbSnS$_2$ QDs/ KI$_3$/I$_3^-$/Graphite/ITO quantum dot sensitized solar cell

Solar cell	Voc	Jsc	FF	η
ITO/TiO$_2$/PbSnS$_2$ QDs/ KI$_3$/I$_3^-$/Graphite/ITO	1.235 V	0.1mA/cm^2	0.2526	0.031%

Field dependence was studied from the $V^{1/2}$ – log(J/V^2) graph but the solar cell was found to be field independent as shown in figure 18.

Figure 18: Zero field dependence of SCLC region for PTS sensitized solar cell

5. **Synthesis and Characterization of Lead Zinc Tin Sulphide quantum dot thin films and J-V characteristics of its solar cell:** Since there is no information regarding the synthesis of lead zinc tin sulphide (PZTS) in literature, we have used VESTA software to draw its structure by using the crystallographic information file of CZTS and replacing the Cu atoms with Pb atoms. The simulated crystal structure of PZTS is shown in figure 7.19. The crystal has a hexagonal structure belonging to space group P1 with lattice constants a=b= 5.46350 Å, c= 10.90420 Å, α= β= γ= 90° and cell volume of 325.4885 Å^3.
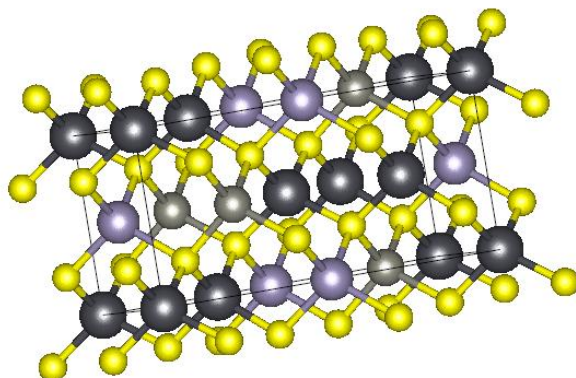

Figure 9: Simulated crystal structure of PZTS. Light grey spheres indicate Zn atoms, dark grey spheres indicate Pb atoms, violet spheres indicate Sn atoms and yellow spheres show S atoms.

The XRD pattern, also simulated from VESTA software has been shown in figure 20. The experimental diffraction pattern of SILAR deposited PZTS quantum do thin film was found to match well with the simulated pattern with slight variations in 2θ values owing to quantum confinement effects. The XRD pattern obtained experimentally has been shown in figure 21. Broad peaks confirm the presence of nanosized particles. There are diffractions at 29.8° and at 41.37° corresponding to (112) and (114) planes. Crystallite size was calculated from the most preferred orientation (112) and the value was calculated to be 0.814nm and so the quantum dot thin film that we have prepared is in the strong confinement regime. Due to the nanosized particles, the lattice strain and dislocation density are higher with values of 9.385 and 1.509 nm^{-2} respectively. The crystal parameters have been tabulated in table 11.
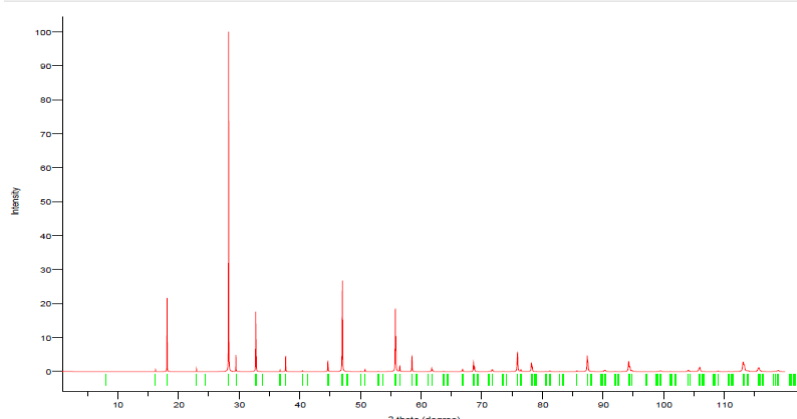
Figure 20: Simulated XRD pattern
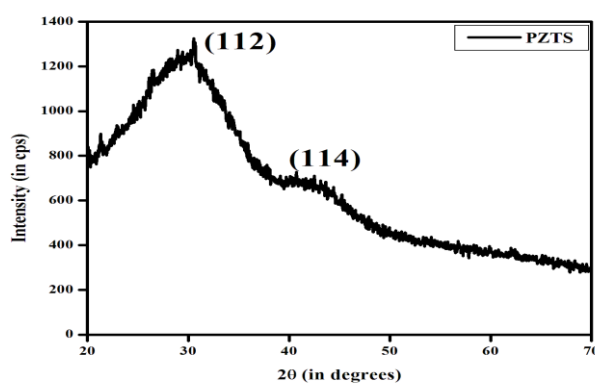
Figure 21: XRD pattern of PZTS quantum dot thin film

**Table 11: Crystal parameters of PZTS quantum dot thin films**

Most preferred orientation	FWHM (radians)	Crystallite size	Lattice Strain	Dislocation density
(112)	0.1704	0.814 nm	9.385	1.509 nm^{-2}

The plot of absorption coefficient vs wavelength has been shown in figure 22. The PZTS quantum dot thin film has high absorption coefficient of 10^6 m^{-1} in the ultraviolet region i.e., from 200 nm to 330 nm and 10^5 m^{-1} in the visible and infrared regions. Thus this material also has promising applications in photovoltaics. There are multiple absorption peaks as it is a highly confined structure. Bandgap for the quantum dot thin film was found from Tauc plot shown in figure 22 and it has been found to be around 4.0 eV.

The cross- sectional Scanning Electron Microscopy (SEM) image of PZTS quantum dot thin film is shown in figure 23. Good quality thin film of thickness of 585.9 nm has been found from the image.

(a)   (b)
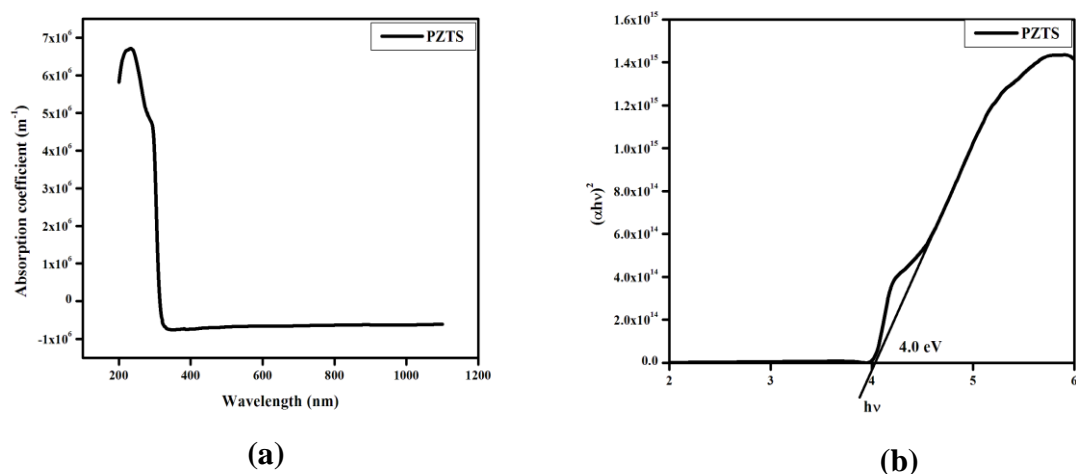
**Figure 22. Absorption coefficient curve
and (b) Tauc plot of PZTS quantum dot thin film**
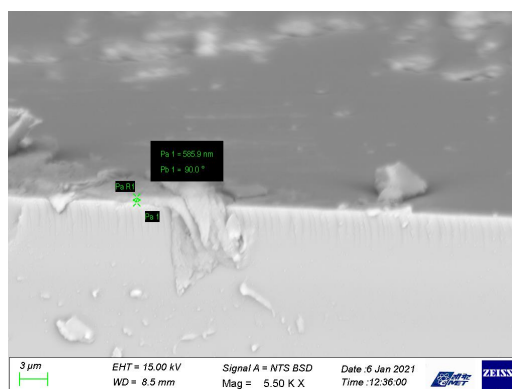
Figure 23: Cross- sectional SEM image of PZTS quantum dot thin film

Hall effect measurement was made on the PZTS quantum dot thin film and it was found to be p-type semiconducting in nature with hole mobility of 18.77 cm^2/Vs, bulk concentration of 1.26 X 10^{11} cm^{-3} and average hole coefficient of 4.95 X 10^7 cm^3/C.

The current obtained from this solar cell is very small, in the range of nanoamperes and picoamperes and so the solar cell parameters were not calculated. Very low efficiencies would be obtained from such a cell.

6. **Simulation of quantum dot sensitized solar cells using SCAPS-1D software**: Using the values of band gap and carrier mobility the simulation of the quantum dot sensitized solar cells was done using SCAPS-1D software under the standard illumination condition of AM 1.5G. Quantum dots of Cu_2S, Cu_2SnS_3 and Cu_2ZnSnS_4 were used as the sensitizer materials, graphite as the counter electrode, iodide/triiodide mixture as the redox couple or electrolyte and TiO_2 as the electron transporting layer. Al was used as the back contact with the metal work function of 4.26eV [20]. The structure of the simulated quantum dot sensitized solar cell structure is shown in figure 24.
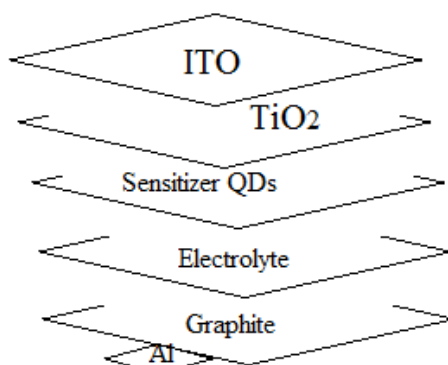
Figure 24: Simulated solar cell structure

The parameters taken from literature [21- 25] and experimental data are tabulated in table 12.

Table 12: Parameters used in the simulation
(Refered below)

Simulation of Cu₂S quantum dot sensitized solar cells: The band diagram and I-V curve of Cu2S quantum dot sensitized solar cell is shown in figure 7.25. Simulations were performed where the band gap of the sensitizer (Cu$_2$S quantum dot) was varied and the efficiencies were obtained, the variation of which is shown graphically in figure 26.
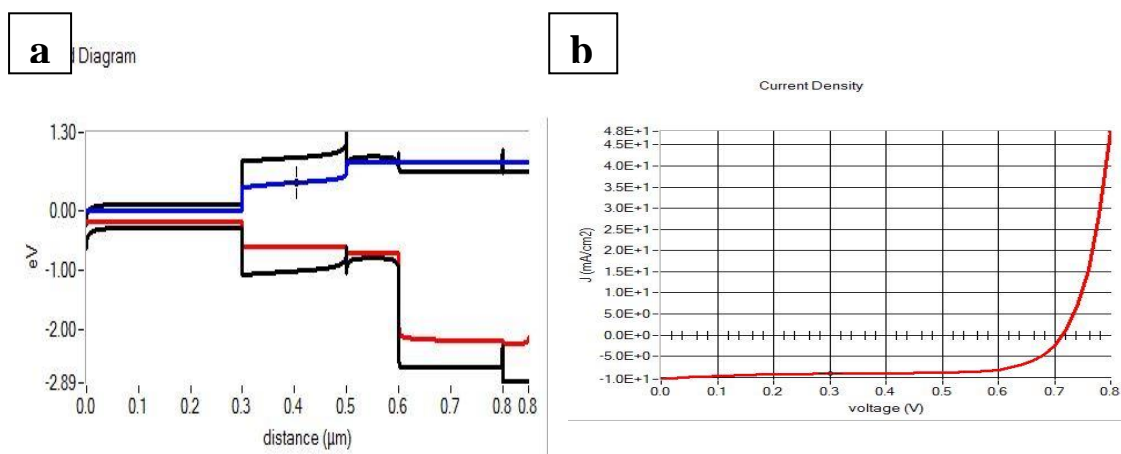
Figure 25: (a) Band diagram and (b) I-V curve of Cu₂S quantum dot
Sensitized solar cell

The efficiency of the solar cell decreases as the band gap of the sensitizer material increases. This is because of the fact that as the band gap of the sensitizer material increases, the number of photoelectrons decreases as only few high energy photons can excite the charge carriers resulting in lower short circuit current and thereby lower efficiency.
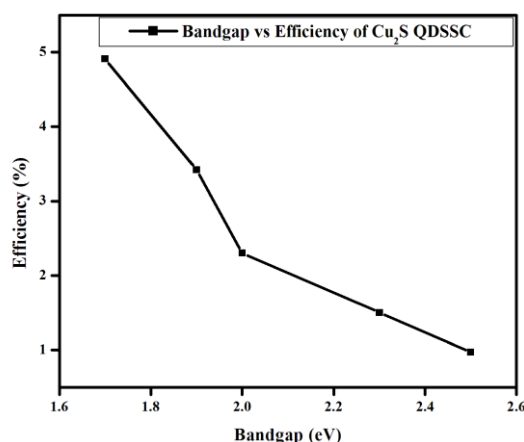
Figure 26: Variation of efficiency with bandgap

Then, the thickness of the sensitizer material was changed in steps of 0.2μm and its effect on the efficiency of the solar cells was investigated. The variation has been shown graphically in figure 27.
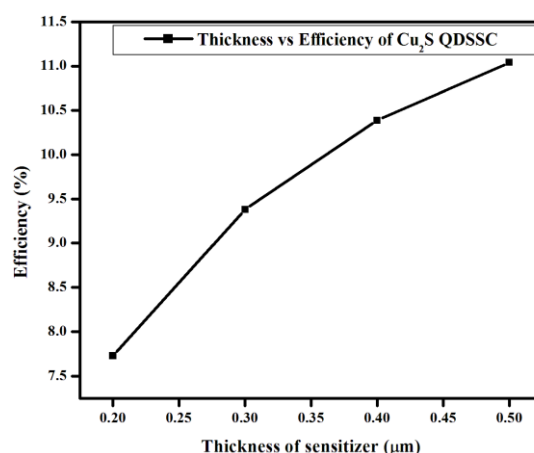

Figure 27: Variation of efficiency with thickness of sensitizer

Considerable increase in band gap of the solar cells was found when the thickness of the sensitizer was increased. On doubling the thickness, the efficiency increased by 1.5 times. Increasing the thickness of the sensitizer increases the photon absorption, increasing the short circuit current and thereby increasing the efficiency of the solar cells. The effect of varying the thickness of the counter electrode, graphite layer was also studied. There is hardly any change in the efficiency of the solar cells when the thickness of the counter electrode was increased upto 1μm. The counter electrode has no role in the production of photoelectrons which directly influences the efficiency of the solar cells.

**Simulation of Cu_2SnS_3 quantum dot sensitized solar cells :** The energy band diagram and the J-V curve of CTS quantum dot sensitized solar cell is shown in figure 28.
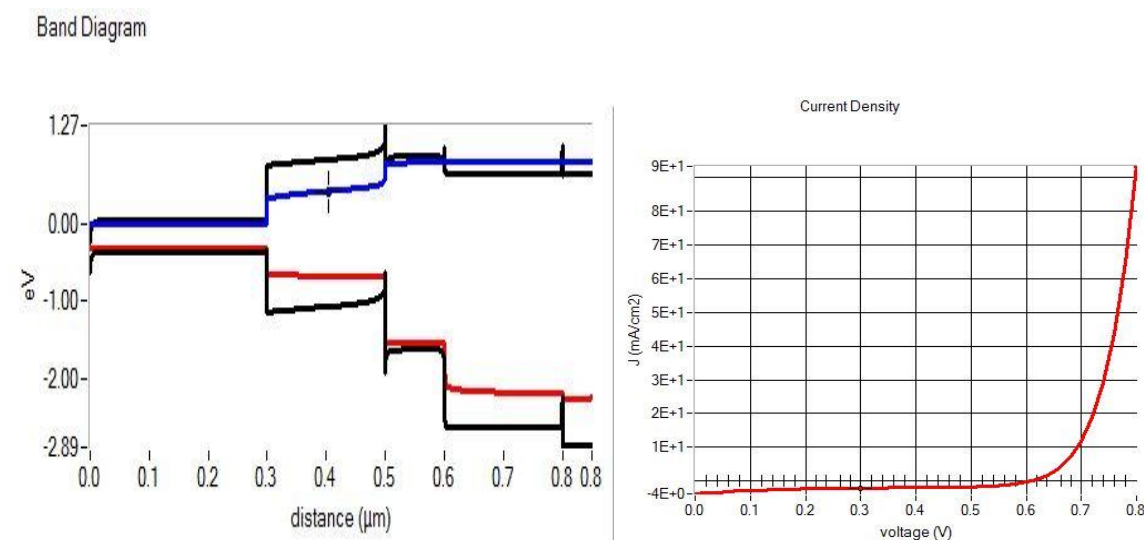
Figure 28: I-V curve of CTS QDSSC

The bandgap of the sensitizer was increased and then decreased and it effect on the efficiency of the solar cell was studied. The variation has been shown graphically in figure 29.
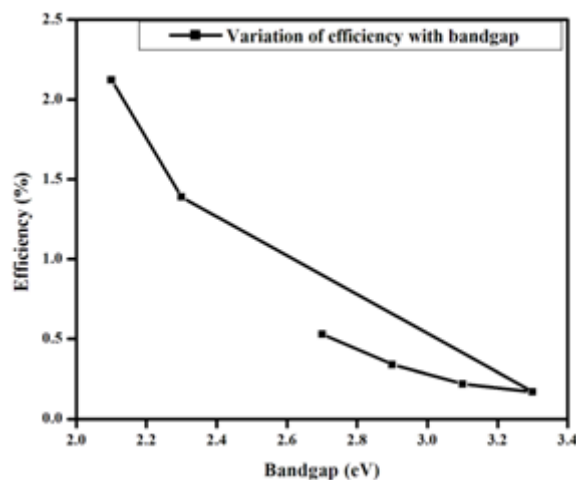
Figure 29: Variation of efficiency with bandgap

As the band gap of the sensitizer was increased, the short circuit current density decreased because only lower number of photoelectrons would be generated owing to the high band gap. The efficiency of the solar cells decreased much as the short circuit current density decreased. The efficiency increased as the band gap was decreased. The efficiency increased considerably as the band gap approached the bulk band gap. The effect of thickness of the sensitizer material on the efficiency of the solar cell was studied. The thickness of the sensitizer was increased by 0.1nm and the solar cell efficiency increased gradually. Even at micron thickness, the efficiency reached only 2.78%. Higher efficiency could be effectively tuned by changing the band gap rather than tuning the thickness of the sensitizer material. Although higher thickness of the sensitizer increases

the number of photoelectrons, it can also increase the possibility of recombination and so the efficiency always remains lower. The findings are shown graphically in figure 30.
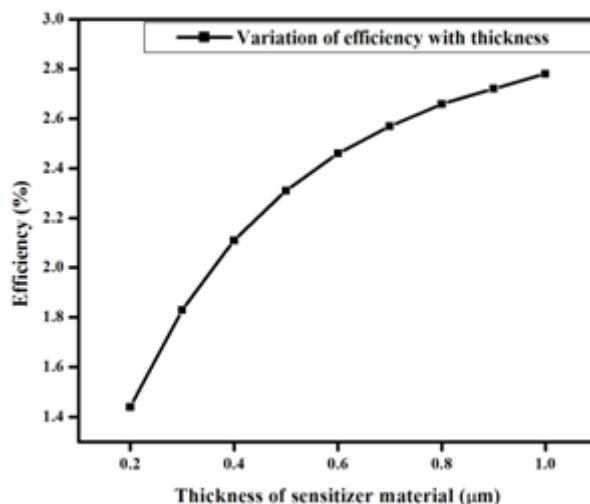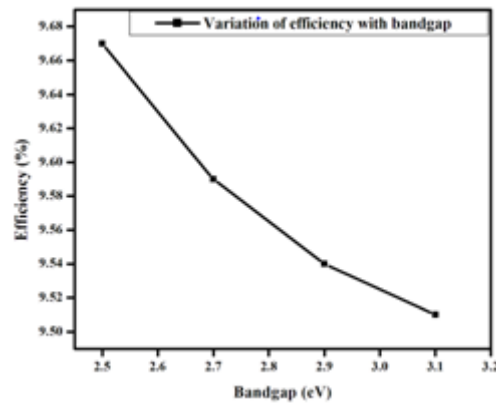

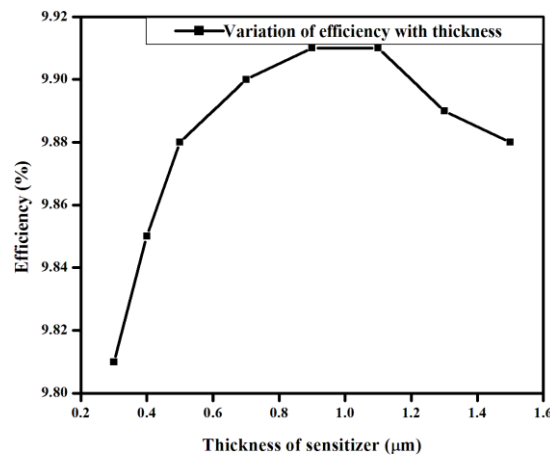**Figure 30: Variation of efficiency with thickness of sensitizer material**

The thickness of the counter electrode, graphite was increased and decreased to study its effect on the efficiency of the solar cell and it was found that the efficiency remained almost the same at different thickness. The thickness of graphite layer was found to have no influence on the efficiency of solar cells. These simulations were performed with n-type of CTS. Simulations were performed with p-type CTS too and the same results were obtained. The type of the sensitizer material does not have any effect on the efficiency of a quantum dot sensitized solar cell.

Simulation of Cu_2SnS_3 quantum dot sensitized solar cells with Cu_2S as counter electrode : Simulations were performed with Cu_2S as the counter electrode and Cu_2SnS_3 as the sensitizer material. The parameters taken were same as given in table 7.4. The bandgap of the sensitizer (CTS) was changed and the variation in efficiency of solar cells was investigated. The variation has been shown graphically in figure 31.

Similar to the previous cases, the thickness of the sensitizer was increased upto few microns and the efficiency of the solar cell were found to increase slightly as shown in figure 7.32. Considerably good efficiencies could be obtained with Cu_2SnS_3 as the sensitizer material and Cu_2S as the counter electrode.

Figure 31: Variation of efficiency with band gap of the sensitizer material.

Figure 32: Variation of efficiency with thickness of the sensitizer

Simulation of Cu$_2$ZnSnS$_4$ quantum dot sensitized solar cells: Similarly, simulations were performed with CZTS as the sensitizer material. Both band gap and thickness of the sensitizer were varied and observations similar to the previous cases were obtained. The I-V curve and energy band diagrams are shown in figure 7.33. The variations in efficiency due to change in bandgap and thickness of sensitizer have been shown graphically in figure 34. The increase in efficiency is slow and saturates when the thickness of the sensitizer reaches the micron range.

Figure 33: (a) Energy band diagram and (b) I-V curve of CZTS QDSSC
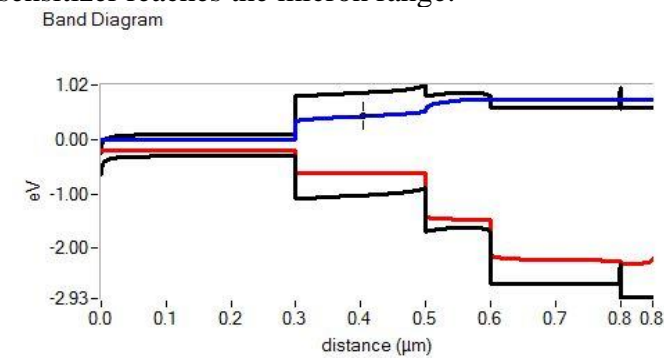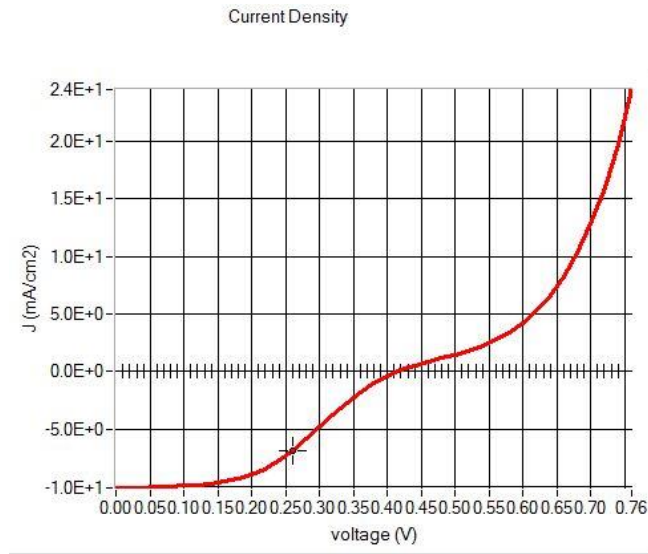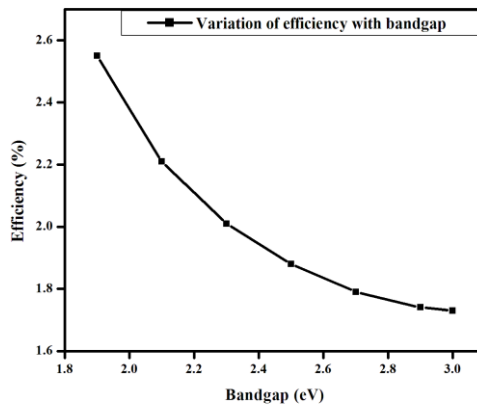

Figure 34: Variation of efficiency with band gap of sensitizer

Figure 35: Variation of efficiency with thickness of the sensitizer

IV. CONCLUSION

Through this work we have achieved in fabricating cost effective quantum dot sensitized solar cells of binary, ternary and quaternary copper and lead chalcogenides. We also calculated the mobility of charge carriers from the dark characteristi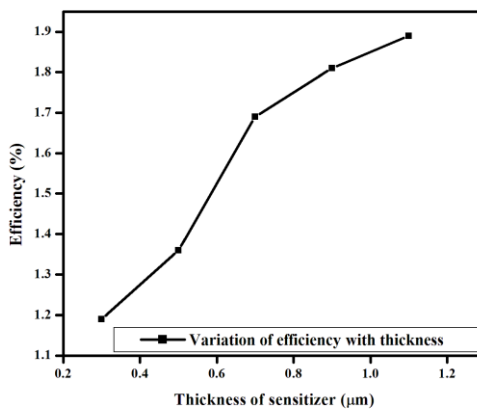cs as these devices had negative field dependence in the steady state space charge limited conduction regime. The devices have fairly good efficiencies due to the considerable charge carrier mobilities. Simulation was performed on the quantum dot sensitized solar cells of Cu_2S, CTS and CZTS. The variation of efficiency with band gap and thickness of the sensitizer were studied. Investigations were also made theoretically on the possibilities of fabricating the above mentioned quantum dot sensitized solar cells using Cu_2S as the photocathode.

REFERENCES

[1] Alizadeh A, Roudgar-Amoli M, Bonyad-Shekalgourabi SM, Shariatinia Z, Mahmoudi M, Saadat F. Dye sensitized solar cells go beyond using perovskite and spinel inorganic materials: A review. Renewable and Sustainable Energy Reviews. 2022 Apr 1;157:112047.

[2] Britel O, Fitri A, Benjelloun AT, Slimi A, Benzakour M, Mcharfi M. Theoretical investigation of the influence of π-spacer on photovoltaic performances in carbazole-based dyes for dye-sensitized solar cells applications. Journal of Photochemistry and Photobiology A: Chemistry. 2022 Feb 23:113870.

[3] Venkatesan S, Lin WH, Hsu TH, Teng H, Lee YL. Indoor Dye-Sensitized Solar Cells with Efficiencies Surpassing 26% Using Polymeric Counter Electrodes. ACS Sustainable Chemistry & Engineering. 2022 Feb 8.

[4] Amani-Ghadim AR, Mohammad-Gholipour-Rezaei E, Bayat F, Agbolaghi S, Khodam F. Enhancement in photovoltaic properties of exciplex quantum dot sensitized solar cells via gadolinium doping and formation of type II Core/Shell (Gd-doped CdS@ CdSe) structure. Solar Energy. 2022 Jan 1;231:402-13.

[5] Markna JH, Rathod PK. Review on the efficiency of quantum dot sensitized solar cell: Insights into photoanodes and QD sensitizers. Dyes and Pigments. 2022 Jan 14:110094.

[6] Monika S, Mahalakshmi M, Veerathangam K, Senthil Pandian M, Ramasamy P. Conductive carbon black/CuS composite counter electrode for the enhanced photovoltaic performance of CdS quantum dot sensitized solar cells. Applied Physics A. 2022 Mar;128(3):1-3.

[7] Rizwan M, Mingsukang MA, Akhtaruzzaman M. Quantum dot-sensitized solar cells. InComprehensive Guide on Organic and Inorganic Solar Cells 2022 Jan 1 (pp. 245-271). Academic Press.

[8] Rühle S, Shalom M, Zaban A. Quantum-dot-sensitized solar cells. ChemPhysChem. 2010 Aug 2;11(11):2290-304.

[9] Huang D, Peng Z, Long C, Luo W, Wang Y, Fu Y. Inorganic iodide surface passivation on PbS quantum dots by one-step process for quantum dots sensitized solar cells. Chemical Physics Letters. 2022 Jan 24:139406.

[10] Zhao Q, Han R, Marshall AR, Wang S, Wieliczka BM, Ni J, Zhang J, Yuan J, Luther JM, Hazarika A, Li GR. Colloidal Quantum Dot Solar Cells: Progressive Deposition Techniques and Future Prospects on Large-area Fabrication. Advanced Materials. 2022 Jan 13:2107888.

[11] Koralay H, TUĞLUOĞLU N, AKGÜL K, ÇAVDAR Ş. Analysis of hopping conduction and space charge limited currents in nearly ideal metal/semiconductor contacts. Gazi University Journal of Science. 2014 Jan 1;27(3):901-7.

[12] Bhutta MS, Akram S, Meng P, Castellon J, Agnel S, Li H, Guo Y, Rasool G, Hussain S, Nazir MT. Steady-state conduction current performance for multilayer polyimide/SiO2 films. Polymers. 2021 Jan;13(4):640.

[13] Chiu FC. A review on conduction mechanisms in dielectric films. Advances in Materials Science and Engineering. 2014 Feb 18;2014.

[14] Bhattarai G, Caruso AN, Paquette MM. Steady-state space-charge-limited current analysis of mobility with negative electric field dependence. Journal of Applied Physics. 2018 Jul 28;124(4):045701.

[15] Mathew M, Preetha KC. Effect of Pelargonidin on carrier recombination lifetime of CTS quantum dots. Optik. 2020 Mar 1;205:164275.

[16] Mathew M, Preetha KC. Mesoporous copper tin sulphide quantum dots as photoanode materials for efficient dye-sensitized solar cell. Optik. 2020 Dec 1;224:165411.

[17] Lu X, Zhuang Z, Peng Q, Li Y. Wurtzite Cu 2 ZnSnS 4 nanocrystals: a novel quaternary semiconductor. Chemical Communications. 2011;47(11):3141-3.

[18] Singh S, Katiyar AK, Midya A, Ghorai A, Ray SK. Superior heterojunction properties of solution processed copper-zinc-tin-sulphide quantum dots on Si. Nanotechnology. 2017 Oct 2;28(43):435704.

[19] Soriano RB, Malliakas CD, Wu J, Kanatzidis MG. Cubic Form of Pb2–x Sn x S2 Stabilized through Size Reduction to the Nanoscale. Journal of the American Chemical Society. 2012 Feb 15;134(6):3228-33.

[20] Eastment RM, Mee CH. Work function measurements on (100),(110) and (111) surfaces of aluminium. Journal of Physics F: Metal Physics. 1973 Sep 1;3(9):1738.

[21] Sawicka-Chudy P, Starowicz Z, Wisz G, Yavorskyi R, Zapukhlyak Z, Bester M, Sibiński M, Cholewa M. Simulation of TiO2/CuO solar cells with SCAPS-1D software. Materials Research Express. 2019 Jun 19;6(8):085918.

[22] Rahman MA. Design and simulation of a high-performance Cd-free Cu2SnSe3 solar cells with SnS electron-blocking hole transport layer and TiO2 electron transport layer by SCAPS-1D. SN Applied Sciences. 2021 Feb;3(2):1-5.

[23] Wells B. Nanostructured Device Designs for Enhanced Performance in CdS/Cu 2 S Heterojunction Solar Cells.

[24] Xosrovashvili G, Gorji NE. Numerical analysis of TiO2/Cu2ZnSnS4 nanostructured PV using SCAPS-1D. Journal of Modern Optics. 2013 Jun 1;60(11):936-40.

[25] Mehrabian M, Dalir S. Numerical simulation of highly efficient dye sensitized solar cell by replacing the liquid electrolyte with a semiconductor solid layer. Optik. 2018 Sep 1;169:214-23.

Table 12: Parameters used in the simulation

Parameter	ITO	TiO2	Quantum Dots			Electrolyte	Graphite
			Cu2S	CTS	CZTS		
Thickness (μm)	0.05	0.2	0.1	0.1	0.1	0.2	0.3
Bandgap	3.5	3.26	1.7	2.5	2.5	1.9	0.4
Electron affinity	4.6	4.20	4.45	4.5	4.0	3.79	4.5
Dielectric constant	8.9	10	30	10	13	3.5	10
Density of states in the conduction band	2.2×10^{18}	2.0×10^{17}	10^{19}	10^{19}	7.5×10^{19}	6.02×10^{21}	10^{18}
Density of states in the valence band	1.8×10^{19}	6×10^{17}	10^{19}	10^{19}	1.8×10^{19}	6.02×10^{21}	10^{18}
Thermal velocity of electrons	10^7	1×10^7	1×10^7	1×10^7	1×10^7	1×10^7	1×10^7
Thermal velocity of holes	1×10^7	1×10^7	1×10^7	1×10^7	1×10^7	1×10^7	1×10^7
Electron mobility	10	100	1.912×10^{-3}	5×10^{-4}	3.774×10^{-4}	0.1	1.8×10^3
Hole mobility	10	25	1.912×10^{-3}	5×10^{-4}	3.774×10^{-4}	0.3	1×10^3
Density of donor atoms	10^{21}	10^{20}	0	10^{15}	0	10^{18}	10^3
Density of acceptor atoms	0	0	10^{16}	0	7×10^{15}	10^{18}	10^3